

Distributed control for geometric pattern formation of large-scale multirobot systems

Andrea Giusti ^{*1}, Gian Carlo Maffettone ^{*2}, Davide Fiore³, Marco Coraggio², and Mario di Bernardo ^{†1,2}

¹*Department of Electrical Engineering and Information Technology, University of Naples Federico II, Via Claudio 21, Naples, 80125, Italy*

²*Scuola Superiore Meridionale, School for Advanced Studies, Largo S. Marcellino, 10, Naples, 80138, Italy*

³*Department of Mathematics and Applications “R. Caccioppoli”, University of Naples Federico II, Via Cintia, Monte S. Angelo, Naples, 80126, Italy*

Keywords multiagent systems, geometric pattern formation, distributed control, swarm robotics

Abstract

Geometric pattern formation is crucial in many tasks involving large-scale multi-agent systems. Examples include mobile agents performing surveillance, swarm of drones or robots, or smart transportation systems. Currently, most control strategies proposed to achieve pattern formation in network systems either show good performance but require expensive sensors and communication devices, or have lesser sensor requirements but behave more poorly. Also, they often require certain prescribed structural interconnections between the agents (e.g., regular lattices, all-to-all networks etc). In this paper, we provide a distributed displacement-based control law that allows large group of agents to achieve triangular and square lattices, with low sensor requirements and without needing communication between the agents. Also, a simple, yet powerful, adaptation law is proposed to automatically tune the control gains in order to reduce the design effort, while improving robustness

and flexibility. We show the validity and robustness of our approach via numerical simulations and experiments, comparing it with other approaches from the existing literature.

1 Introduction

1.1 Problem description and motivation

Many robotic applications require—or may benefit from—one or more groups of multiple agents to perform a joint task [1]; this is, for example, the case of surveillance, exploration, herding [2] or transportation [3]. When the number of agents becomes extremely large, the task becomes a *swarm robotics* problem [4]. Typically, in these problems, it is assumed that the agents are relatively simple, and thus have limited communication and sensing capabilities, and limited computational resources; see for example the robotic swarms described in [5, 6, 7].

In swarm robotics, typical tasks of interest include *aggregation, flocking, foraging, object clustering, navigation, spatial organisation, collaborative manipulation*, and *task allocation* [4, 3]. Among these, an important subclass of spatial organisation problems is

^{*}These authors contributed equally to this work.

[†]Corresponding Author

geometric pattern formation, where the goal is for the agents to self-organize their relative positions into some desired structure or *pattern*, e.g., multiple adjacent triangles. Pattern formation is crucial in many applications [8], including sensor networks deployment [9, 10], collective search and rescue [11, 12], collective transportation and construction [13, 14], and 3D-2D exploration and mapping [15]. There are two main difficulties associated with achieving pattern formation. Firstly, as there are no leader agents, the pattern must emerge by exploiting a control strategy that is the same for all agents, *distributed* and *local* (i.e., each agent can only use information about “nearby” agents). Secondly, the number of agents is large and may change over time; therefore the control strategy must also be *robust* to uncertainties in the size of the swarm and to its possible variations.

This sets the problem of achieving pattern formation apart from the more classical *formation control* problems [16] where agents are typically fewer and have pre-assigned roles within the formation.

Nevertheless, some of the theory and solutions developed for formation control may be exploited to describe pattern formation. For this reason, to classify existing solutions to pattern formation, we employ the same taxonomy proposed in [16] for formation control, which is based on the type of information available to the agents. Namely, existing strategies can be classified as being (i) *position-based* when it is assumed agents know their position and orientation and those of their neighbours, in a global reference frame; (ii) *displacement-based* when agents can only sense their own orientation with respect to a global reference direction (e.g., North) and the relative positions of their neighbours; (iii) *distance-based* when agents can measure the relative positions of their neighbours with respect to their local reference frame. In terms of sensor requirements, position-based solutions are the most demanding, requiring global positioning sensors, typically GPS, and communication devices, such as WiFi or LoRa. Differently, displacement-based methods require only a distance sensor (e.g., LiDAR) and a compass, although the latter can be replaced by a coordinated initialisation procedure of all local reference frames [17]. Finally, distance-based algorithms are the less demand-

ing, needing only some distance sensors.

A pressing open challenge in pattern formation problems is devising new control strategies that can combine low sensor requirements with high and consistent performance. This is crucial in swarm robotics, where it would be cumbersome or prohibitively expensive to equip all agents with GPS sensors and communication capabilities.

1.2 Related work

Position-based approaches

In [18], a position-based algorithm was proposed to achieve 2D triangular lattices in a constellation of satellites in a 3D space. This strategy combines global attraction towards a reference point with local interaction among the agents to control both the global shape and the internal lattice structure of the swarm. In [19], a position-based approach was presented that combines the common radial virtual force (also used in [20, 21, 22, 23]) with a normal force. In this way, a network of connections is built such that each agent has at least two neighbours; then, a set of geometric rules is used to decide whether any or both of these forces are applied between any pair of agents. Importantly, this approach requires the acquisition of positions from two-hop neighbours. In [9], a position-based strategy is presented to achieve triangular and square patterns, as well as lines and circles, both in 2D and 3D; the control strategy features global attraction towards a reference point and re-scaling of distances between neighbours, with the virtual forces changing according to the goal pattern. A qualitative comparison was also provided with the distance-based strategy from [21], showing more precise configurations and a shorter convergence time, due to the position-based nature of the solution.

Displacement-based approaches

In [24], a displacement-based approach is presented based on the use of a geometric control law similar to the one proposed in [25]. The aim is to obtain triangular lattices but small persisting oscillations of the agents are present at steady state, as the robots

are assumed to have a constant non-zero speed. In [26, 27], an approach is discussed inspired by covalent bonds in crystals, where each agent has multiple attachment points for its neighbours. Only starting conditions close to the desired pattern are tested, as the focus is on navigation in environments with obstacles. Finally, in [28] the desired lattice is encoded by a graph, where the vertices denote possible *roles* the agents may play in the lattice and edges denote rigid body transformations between the local frames or reference of pairs of neighbours. All agents communicate with each other and are assigned a label (or identification number) through which they are organised hierarchically to form triangular, square, hexagonal or octagon-square patterns.

Distance-based approaches

A popular distance-based approach for the formation of triangular and square lattices, named *physicomimetics*, was proposed in [20] and later also studied in [21, 22]. The control strategy is based on the use of *virtual forces* [29], an approach inspired by Physics, where each agent is subject to virtual forces (e.g., Lennard-Jones and Morse functions [4, 30]) from neighbouring agents, obstacles, and the environment. In these studies ([20, 21, 22]), triangular lattices are achieved with long-range attraction and short-range repulsion forces only, while square lattices are obtained through a selective rescaling of the distances between some of the agents. An extension for the formation of hexagonal lattices was proposed in [31], but with the requirement of an ad hoc correction procedure to prevent agents from remaining stuck in the centre of a hexagon. The main drawback of the physicomimetics strategy ([20, 21, 22, 31]) is that it can produce the formation of multiple aggregations of agents, each respecting the desired pattern, but with different orientations. Another problem, described in [21], is that, for some values of the parameters, multiple agents can converge towards the same position and collide. In [23], an approach exploiting Lennard-Jones-like virtual forces is numerically optimised to stabilise locally a hexagonal lattice. When applied to mobile agents, the interaction law is time-varying and requires synchronous clocks among

the agents. In [25], a different distance-based control strategy, derived from geometric arguments, was proposed to achieve the formation of triangular lattices. In this study, an analytical proof of convergence to the desired lattice is given exploiting Lyapunov methods. Robustness to agents' failure and the capability of detecting and repairing holes and gaps in the lattice are obtained via an ad hoc procedure and verified numerically. A 3D extension was later presented in [32].

1.3 Contribution

In this paper, we introduce a *distributed displacement-based* control strategy to solve pattern formation problems in swarm robotics that requires no communication among the agents or labelling them. In particular, to achieve triangular and square lattices we employ two virtual forces controlling the norm and the angle of their relative position, respectively. The main contributions can be listed as follows

1. Our strategy performs significantly better than other distance-based algorithms ([20, 31]) when achieving square lattices, in terms of precision and robustness, with only a minimal increase in sensor requirements (a compass) and without needing the more costly sensors and communication devices used for position-based strategies.
2. The control gains can be set automatically, according to a simple adaptive law, in order for the agents to organize themselves and switch from one pattern to the other.
3. Numerical simulations and experiments show its effectiveness even in the presence of actuator constraints and other more realistic effects.

2 Preliminaries

Notation

We denote by $\|\cdot\|$ the Euclidean norm. Given a set \mathcal{B} , its cardinality is denoted by $|\mathcal{B}|$. We refer to \mathbb{R}^2 as the *plane*.

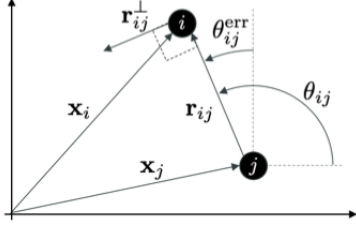


Figure 1: Geometrical relationship between a pair of agents.

2.1 Planar swarms

Definition 1 (Swarm) A (planar) swarm $\mathcal{S} := \{1, 2, \dots, N\}$ is a set of $N \in \mathbb{N}_{>0}$ identical agents that can move on the plane. For each agent $i \in \mathcal{S}$, $\mathbf{x}_i(t) \in \mathbb{R}^2$ denotes its position in the plane at time $t \in \mathbb{R}$.

Moreover, $\mathbf{r}_{ij}(t) := \mathbf{x}_i(t) - \mathbf{x}_j(t) \in \mathbb{R}^2$ is the relative position of agent i with respect to agent j , and $\theta_{ij}(t) \in [0, 2\pi]$ is the angle between \mathbf{r}_{ij} and the horizontal axis (see Fig. 1).

Definition 2 (Neighbourhood) Given a swarm and a sensing radius $R_s \in \mathbb{R}_{>0}$, the neighbourhood of agent i at time t is

$$\mathcal{N}_i(t) := \{j \in \mathcal{S} \setminus \{i\} : \|\mathbf{r}_{ij}(t)\| \leq R_s\}. \quad (1)$$

Definition 3 (Adjacency set) Given a swarm and some finite $R_{\min}, R_{\max} \in \mathbb{R}_{>0}$, with $R_{\min} \leq R_{\max}$, the adjacency set of agent i at time t is (see Fig. 2)

$$\mathcal{A}_i(t) := \{j \in \mathcal{S} \setminus \{i\} : R_{\min} \leq \|\mathbf{r}_{ij}(t)\| \leq R_{\max}\}. \quad (2)$$

Notice that if $R_{\max} \leq R_s$ then $\mathcal{A}_i \subseteq \mathcal{N}_i$.

Definition 4 (Links) A link is a pair $(i, j) \in \mathcal{S} \times \mathcal{S}$ such that $j \in \mathcal{A}_i(t)$ (or equivalently $i \in \mathcal{A}_j(t)$). Moreover, $\mathcal{E}(t)$ is the set of all links existing at time t .

Clearly, it is possible to associate to the swarm a time-varying graph $\mathcal{G}(t) = (\mathcal{S}, \mathcal{E}(t))$ [33]; \mathcal{S} and $\mathcal{E}(t)$ being the set of vertices and edges, respectively.¹

¹Formally, $\mathcal{G}(t)$ is a directed graph, even though $\mathcal{E}(t)$ is such that the existence of (i, j) implies the existence of (j, i) .

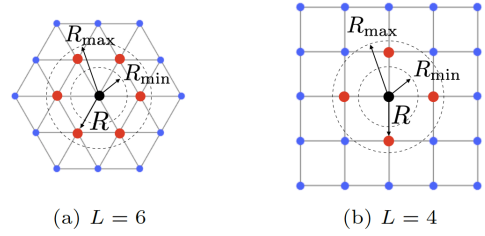


Figure 2: (L, R) -lattice formations for (a) triangular ($L = 6$) and (b) square ($L = 4$) lattices. Red dots are agents in the adjacency set \mathcal{A}_i of the black agent (i) .

Finally, given any two links (i, j) and (h, k) , we denote with $\theta_{ij}^{hk}(t) \in [0, 2\pi]$ the absolute value of the angle between the vectors \mathbf{r}_{ij} and \mathbf{r}_{hk} .

2.2 Lattice and performance metrics

Definition 5 (Lattice) Given some $L \in \{4, 6\}$ and $R \in \mathbb{R}_{>0}$, a (L, R) -lattice is a set of points in the plane that coincide with the vertices of an associated regular tiling [34, 35]; R is the distance between adjacent vertices and L is the number of adjacent vertices each point has.

In Definition 5, $L = 4$, and $L = 6$ correspond to square and triangular lattices, respectively, as portrayed in Fig. 2. We say that a swarm *self-organises into a (L, R) -lattice* if (i) each agent has at most L links, and (ii) $\forall (i, j) \in \mathcal{E}$ and $\forall (h, k) \in \mathcal{E}$ it holds that θ_{ij}^{hk} is some multiple of $2\pi/L$. To assess whether a swarm self-organises into some desired (L, R) -lattice, we introduce two metrics.

Definition 6 (Regularity metric) Given a swarm and a desired (L, R) -lattice, the regularity metric $e_\theta(t) \in [0, 1]$ is

$$e_\theta(t) := \frac{L}{\pi} \cdot \theta_{\text{err}}(t), \quad (3)$$

where, omitting the dependence on time,

$$\theta_{\text{err}} := \frac{1}{|\mathcal{E}|^2 - 2|\mathcal{E}|} \sum_{(i,j) \in \mathcal{E}} \sum_{(h,k) \in \mathcal{E}} \min_{q \in \mathbb{Z}} \left| \theta_{ij}^{hk} - q \frac{2\pi}{L} \right|. \quad (4)$$

The regularity metric e_θ , derived from [20], quantifies the incoherence in the orientation of the links in the swarm. In particular, $e_\theta = 0$ when all the pairs of links form angles that are multiples of $2\pi/L$ (which is desirable to achieve the (L, R) -lattice), while $e_\theta = 1$ when all pairs of links have the maximum possible orientation error, equal to π/L . Finally, $e_\theta \approx 0.5$ generally corresponds to the agents being arranged randomly.

Definition 7 (Compactness metric) *Given a swarm and a desired (L, R) -lattice, the compactness metric $e_L(t) \in [0, (N - 1 - L)/L]$ is*

$$e_L(t) := \frac{1}{N} \sum_{i=1}^N \frac{||\mathcal{A}_i(t)| - L|}{L}. \quad (5)$$

The compactness metric e_L measures the average difference between the number of neighbours each agent has and the one they are ought to have in a (L, R) -lattice. e_L is maximum ($e_L = (N - 1 - L)/L$) when all agents are concentrated in a small region, and links exist between all pairs of agents. $e_L = 1$ when all the agents are scattered loosely in the plane, and no links exist between them. Finally, $e_L = 0$ when all the agents have L links (which is desirable to achieve the (L, R) -lattice). It is important to remark that, if the number N of agents is finite, e_L can never be equal to zero, because the agents on the boundary of the group will always have less than L links (Fig. 2). This effect gets less relevant as N increases. Note that a similar metric is also independently defined in [28].

For the sake of brevity, in what follows we will omit dependence on time when that is clear from the context.

3 Control design

3.1 Problem formulation

Consider a planar swarm \mathcal{S} whose agents' dynamics is described by the first order model

$$\dot{\mathbf{x}}_i(t) = \mathbf{u}_i(t), \quad \forall i \in \mathcal{S}, \quad (6)$$

where $\mathbf{x}_i(t)$ was given in Definition 1 and $\mathbf{u}_i(t) \in \mathbb{R}^2$ is some input signal determining the velocity of agent i .² We aim to solve the following control problem.

Problem statement Design some *distributed* feedback control law $\mathbf{u}_i = \mathbf{g}(\{\mathbf{r}_{ij}\}_{j \in \mathcal{N}_i}, L, R)$ to let the swarm self-organise into a desired triangular or square lattice, starting from any set of initial positions in some disk of radius r . Moreover, we require the law to be:

1. *robust* to failures of agents and to noise;
2. *flexible*, allowing dynamic reorganisation into different patterns;
3. *scalable*, allowing the number of agents N to change dynamically.

To assess the self-organising capability of the swarm, we seek to minimise the performance metrics e_θ and e_L (see Definitions 6 and 7).

3.2 Distributed control law

Next, we present a distributed displacement-based control law that solves the problem described in Sec. 3.1. Namely, we set

$$\mathbf{u}_i(t) = \mathbf{u}_{r,i}(t) + \mathbf{u}_{n,i}(t), \quad (7)$$

where $\mathbf{u}_{r,i}$ and $\mathbf{u}_{n,i}$ are the *radial* and *normal* control inputs, respectively. The two inputs have different purposes and each comprises several *virtual forces*. The radial input $\mathbf{u}_{r,i}$ is the sum of attracting/repelling actions between the agents, with the purpose of aggregating them into a compact swarm, while avoiding collisions. The normal input $\mathbf{u}_{n,i}$ is also the sum of multiple actions, used to adjust the angles of the relative positions of the agents.

Law (7) is *displacement-based* because it only requires that each agent i (i) can measure the relative

²First order models like (6) are often used in the literature [25, 32, 19, 9]. In some other works [20, 21, 31] a second order model is used, given by $m\ddot{\mathbf{x}}_i + \mu\dot{\mathbf{x}}_i = \mathbf{u}_i$, where \mathbf{u}_i is a force, m is a mass and μ is a viscous friction coefficient. Under the simplifying assumptions of small inertia ($m\|\dot{\mathbf{v}}_i\| \ll \mu\|\mathbf{v}_i\|$) and $\mu = 1$, the two models coincide.

positions of the agents close to it (in the sets \mathcal{N}_i and \mathcal{A}_i), and (ii) has the knowledge of a common reference direction. Next, we describe in detail the two control actions in (7).

3.3 Radial Interaction

The radial control input $\mathbf{u}_{r,i}$ in (7) is defined as the sum of several virtual forces, one for each agent in \mathcal{N}_i (neighbours of i), each force being attractive (if the neighbour is far) or repulsive (if the neighbour is close). Specifically,

$$\mathbf{u}_{r,i} = G_{r,i} \sum_{j \in \mathcal{N}_i} f_r(\|\mathbf{r}_{ij}\|) \frac{\mathbf{r}_{ij}}{\|\mathbf{r}_{ij}\|}, \quad (8)$$

where $G_{r,i} \in \mathbb{R}_{\geq 0}$ is the radial control gain. Note that $\mathbf{u}_{r,i}$ is termed as *radial* input because in (8) the attraction/repulsion forces are parallel to the vectors \mathbf{r}_{ij} (see Fig. 1). The magnitude and sign of each of these actions depend on the distance ($\|\mathbf{r}_{ij}\|$) between the corresponding agents, according to the *radial interaction function* $f_r : \mathbb{R}_{>0} \rightarrow \mathbb{R}$. Here, we select f_r as the Physics-inspired Lennard-Jones function [4, 22], given by

$$f_r(\|\mathbf{r}_{ij}\|) = \min \left\{ \left(\frac{a}{\|\mathbf{r}_{ij}\|^{2c}} - \frac{b}{\|\mathbf{r}_{ij}\|^c} \right), 1 \right\}, \quad (9)$$

where $a, b \in \mathbb{R}_{>0}$ and $c \in \mathbb{N}$ are design parameters. In (9), f_r is saturated to 1 to avoid divergence for $\|\mathbf{r}_{ij}\| \rightarrow 0$. f_r is portrayed in Fig. 3a.

3.4 Normal Interaction

For any link (i, j) , we define the *angular error* $\theta_{ij}^{\text{err}} \in]-\frac{\pi}{L}, \frac{\pi}{L}[$ as the difference between θ_{ij} and the closest multiple of $2\pi/L$ (see Fig. 1), that is,

$$\theta_{ij}^{\text{err}} := \theta_{ij} - \frac{2\pi}{L} \arg \min_{q \in \mathbb{Z}} \left\{ \left| \theta_{ij} - q \frac{2\pi}{L} \right| \right\}, \quad (10)$$

Then, the normal control input $\mathbf{u}_{n,i}$ in (7) is defined as

$$\mathbf{u}_{n,i} = G_{n,i} \sum_{j \in \mathcal{A}_i} f_n(\theta_{ij}^{\text{err}}) \frac{\mathbf{r}_{ij}^\perp}{\|\mathbf{r}_{ij}\|}, \quad (11)$$

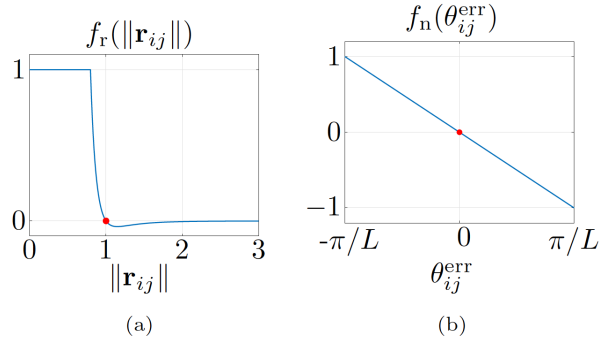


Figure 3: (a) Radial and (b) normal interaction functions. Red dots highlight zeros of the functions. Parameters are taken from Tab 2.

where $G_{n,i} \in \mathbb{R}_{\geq 0}$ is the normal control gain. Each of these actions is applied in the direction of \mathbf{r}_{ij}^\perp , that is the vector normal to \mathbf{r}_{ij} , obtained by applying a $\pi/2$ counterclockwise rotation (see Fig. 1). The magnitude and sign of these forces are determined by the *normal interaction function* $f_n :]-\frac{\pi}{L}, \frac{\pi}{L}[\rightarrow [-1, 1[$, given by

$$f_n(\theta_{ij}^{\text{err}}) = -\frac{L}{\pi} \theta_{ij}^{\text{err}}. \quad (12)$$

f_n is portrayed in Fig. 3b.

We remark that by rotating the axis with respect to which angles θ_{ij} are measured, our algorithm allows to achieve triangular or square lattices with different orientations.

4 Numerical validation

In this section, we assess the performance and the robustness of our proposed control algorithm (7) through an extensive simulation campaign. The experimental validation of the strategy is later reported in Sec. 6. First in Sec. 4.2, using a numerical optimisation procedure, we tune the control gains $G_{r,i}$ and $G_{n,i}$ in (8) and (11), as the performance of the controlled swarm strongly depends on these values. Then in Sec. 4.3, we assess the robustness of the control law with respect to (i) agents' failure and to (ii) noise, (iii) flexibility to pattern change, and (iv)

Table 1: Simulations and experiments

Scenario	Section	Figure(s)
<i>Control law</i> (7),(8),(11)		
Tuning	4.2	4
Validation	4.2	5
Robustness to faults	4.3.1	6
Robustness to noise	4.3.2	7
Flexibility	4.3.3	8
Scalability	4.3.4	9
Comparison with [20, 21]	4.4	10, 11
<i>Adaptive gain tuning</i> (7),(8),(11),(20)		
Validation	5	12
Robustness to faults	5.1.1	13
Flexibility	5.1.2	14
Scalability	5.1.3	15
Robotarium experiment	6	16

scalability. Finally in Sec. 4.4, we present a comparative analysis of our distributed control strategy and other approaches previously presented in the literature. The simulations and experiments performed in this and the next Sections are summarised in Table 1.

4.1 Simulation setup

We consider a swarm consisting of $N = 100$ agents (unless specified differently). To represent the fact that the agents are deployed from a unique source (as typically done in the literature [20, 21]), their initial positions are drawn randomly with uniform distribution from a disk of radius $r = 2$ centred at the origin.³

Initially, for the sake of simplicity and to avoid the possibility of some agents becoming disconnected from the group, we assume that R_s in (1) is large

³That is, denoting with $U([a, b])$ the uniform distribution on the interval $[a, b]$, the initial position of each agent in polar coordinates $\mathbf{x}_i(0) := (d_i, \phi_i)$ is obtained by independently sampling $\phi_i \sim U([0, 2\pi])$ and d_i is chosen according to the probability density function $p_i(\xi) : [0, r] \mapsto \mathbb{R}_{\geq 0}$ defined as $p_i(\xi) = 2\xi/r^2$.

Table 2: Simulation parameters

Parameter	Description	Value
R	Desired link length	1 m
R_{\min}	Minimum link length	0.6 m
R_{\max}	Maximum link length	1.1 m
V_{\max}	Maximum speed	5 m/s
t_{\max}	Maximum simulation time	200 s
Δt	Integration step	0.01 s
T_w	Time window	10 s
a	Radial interaction function $f_r(\cdot)$	0.15
b	"	0.15
c	"	5

enough so that

$$\forall i \in \mathcal{S}, \forall t \in \mathbb{R}_{\geq 0}, \quad \mathcal{N}_i(t) = \mathcal{S} \setminus i; \quad (13)$$

i.e., any agent can sense the relative position of all others. Later, in Sec. 4.3, we will drop this assumption and show the validity of our control strategy also for smaller values of R_s . All simulation trials are conducted in MATLAB⁴, integrating the agents' dynamics using the forward Euler method with a fixed time step $\Delta t > 0$. Moreover, the speed of the agents is limited to $V_{\max} > 0$. The values of the parameters used in the simulations are reported in Tab. 2.

Performance evaluation

To assess the performance of the controlled swarm we exploit the metrics e_θ and e_L given in Definitions 6 and 7. Namely, we select empirically the thresholds $e_\theta^* = 0.2$ and $e_L^* = 0.3$, which are associated to satisfactory compactness and regularity of the swarm. Then, letting $T_w > 0$ be the length of a time window, we say that e_θ is at *steady-state* from time $t' = k\Delta t$ (for $k \in \mathbb{Z}$) if

$$|e_\theta(t') - e_\theta(t' - j\Delta t)| \leq 0.1 e_\theta^*, \quad \forall j \in \left\{ 1, 2, \dots, \left\lfloor \frac{T_w}{\Delta t} \right\rfloor \right\}. \quad (14)$$

⁴The code is available at <https://github.com/diBernardoGroup/SwarmSimPublic>.

We give an analogous definition for the steady state of e_L (using e_L^* rather than e_θ^*). Then, we say that in a trial the swarm *achieved steady-state* at time t_{ss} if there exists a time instant such that both e_θ and e_L are at steady state, and t_{ss} is the smallest of such time instants. Moreover, we deem the trial *successful* if $e_\theta(t_{ss}) < e_\theta^*$ and $e_L(t_{ss}) < e_L^*$. If in a trial steady-state is not reached in the time interval $[0, t_{max}]$, the trial is stopped (and deemed unsuccessful). We define

$$e_\theta^{ss} := \begin{cases} e_\theta(t_{ss}), & \text{if steady state was achieved,} \\ e_\theta(t_{max}), & \text{otherwise.} \end{cases} \quad (15)$$

$$e_L^{ss} := \begin{cases} e_L(t_{ss}), & \text{if steady state was achieved,} \\ e_L(t_{max}), & \text{otherwise.} \end{cases} \quad (16)$$

Finally, to assess how quickly the pattern is formed, we define

$$T_\theta := \min\{t' \in \mathbb{R}_{\geq 0} : e_\theta(t') \leq e_\theta^*, \forall t \geq t'\}, \quad (17)$$

$$T_L := \min\{t'' \in \mathbb{R}_{\geq 0} : e_L(t'') \leq e_L^*, \forall t \geq t''\}. \quad (18)$$

4.2 Tuning of the control gains

For the sake of simplicity, in this section we assume that $G_{r,i} = G_r$ and $G_{n,i} = G_n$, for all $i \in \mathcal{S}$; later, in Sec. 5, we will present an adaptive control strategy allowing each agent to independently vary on-line its own control gains. To select the values of G_r and G_n giving the best performance in terms of regularity and compactness, we conducted an extensive simulation campaign and evaluated, for each pair $(G_r, G_n) \in \{0, 1, \dots, 30\} \times \{0, 1, \dots, 30\}$, the following cost function, averaged over 30 trials, starting with random initial conditions:

$$C(e_\theta^{ss}, e_L^{ss}) = \left(\frac{e_\theta^{ss}}{e_\theta^*}\right)^2 + \left(\frac{e_L^{ss}}{e_L^*}\right)^2. \quad (19)$$

The results are reported in Fig. 4 for the triangular ($L = 6$) and the square ($L = 4$) lattices; in the former case, the pair $(G_r^*, G_n^*)_{L=6}$ minimising C is $(22, 1)$, whereas in the latter case it is $(G_r^*, G_n^*)_{L=4} = (15, 8)$. Both pairs achieve $C \leq 1$, implying $e_\theta^{ss} \leq e_\theta^*$ and $e_L^{ss} \leq e_L^*$.

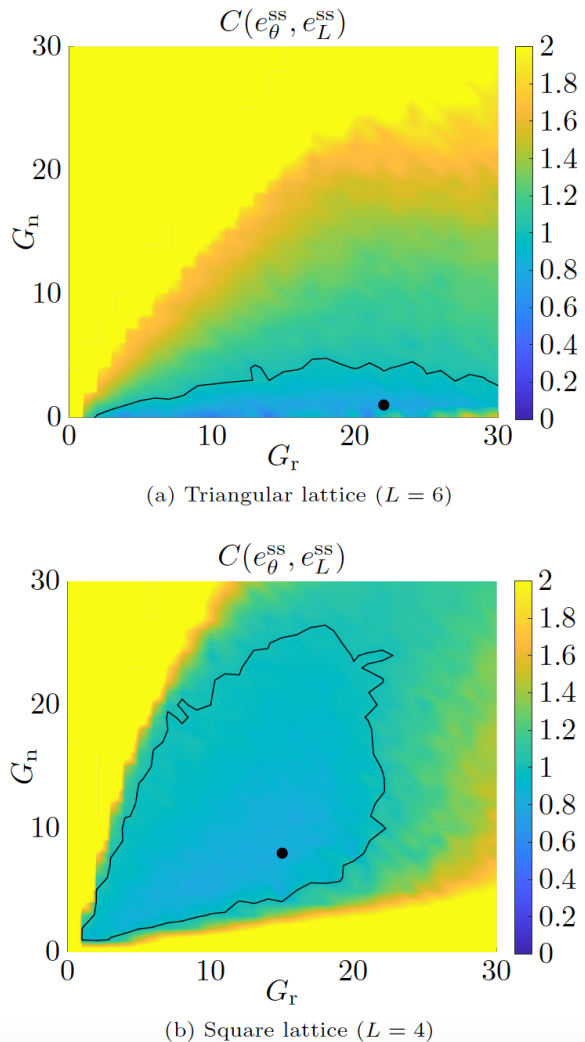


Figure 4: Tuning of the control gains G_r and G_n with (a) $L = 6$ and (b) $L = 4$ (§ 4.2). The black dots correspond to $(G_r^*, G_n^*)_{L=6}$ and $(G_r^*, G_n^*)_{L=4}$, minimising C . The black curves delimit the regions where $C \leq 1$.

In Fig. 5, we report three snapshots at different time instants of two representative simulations, together with the metrics $e_\theta(t)$ and $e_L(t)$, for the cases of a triangular and a square lattice, respectively. The control gains were set to the optimal values $(G_r^*, G_n^*)_{L=6}$ and $(G_r^*, G_n^*)_{L=4}$. In both cases, the metrics quickly converge below their prescribed

thresholds, as $\max\{T_\theta, T_L\} < 2.75$ s. Finally, note that $e_L(t)$ decreases faster than $e_\theta(t)$, meaning that the swarm tends to first reach the desired level of compactness and then agents' positions are rearranged to achieve the desired pattern.

4.3 Robustness analysis

In this section, we investigate numerically the properties that we required in Sec. 3.1, that is robustness to faults and noise, flexibility, and scalability.

4.3.1 Robustness to faults

We ran a series of simulations in which we removed a percentage of the agents at a certain time instant, and assessed the capability of the swarm to recover the desired pattern. For the sake of brevity, we report one of them in Fig. 6, where, with $L = 4$, 30% of the agents were removed at random at time $t = 30$ s. We notice that, as the agents are removed, $e_L(t)$ and $e_\theta(t)$ suddenly increase, but, after a short time, they converge again to values below the thresholds, recovering the desired pattern, despite the formation of small holes that increase e_L^{ss} .

4.3.2 Robustness to noise

We assumed that the dynamics (6) of each agent is affected by additive white Gaussian noise with standard deviation σ . Then, we set $L = 4$ and varied σ in the interval $[0, 1]$ with increments of 0.05. For each value of σ , we ran $M = 30$ trials, starting from random initial conditions, and report the average values of e_θ^{ss} and e_L^{ss} in Fig. 7. We observe that large intensities of noise ($\sigma \geq 0.4$) worsen performance, up to the point of making the trials unsuccessful and preventing the swarm from forming the desired lattice. Interestingly, smaller noise ($0 < \sigma \leq 0.2$) actually improves performance. This is because small random displacements can prevent the agents from getting stuck in undesired configurations, including those containing holes.

4.3.3 Flexibility

In Fig. 8, we report a simulation where L was initially set equal to 4 (square lattice), changed to 6 (triangular lattice) at time $t = 30$ s, and finally changed back to 4 at $t = 60$ s. The control gains are set to $(G_r^*, G_n^*)_{L=4}$ and kept constant during the entire the simulation. Clearly, as L is changed, both e_L and e_θ suddenly increase, but the swarm is quickly able to reorganise and reduce them below their prescribed thresholds in less than 5 s, thus achieving the desired pattern.

4.3.4 Scalability

Before properly testing for scalability, we dropped the assumption that (13) holds and characterised e_L^{ss} as a function of the sensing radius R_s . The results are portrayed in Fig. 9a, showing that the performance starts deteriorating for approximately $R_s < 6$ m, until it becomes unacceptable for about $R_s < 1.1$ m. Therefore, as a good trade-off between performance and feasibility, we set $R_s = 3$ m. To test for scalability, we varied the number N of agents (initially, $N = 100$), reporting the results in Fig. 9b. We see that (i) the controlled swarm correctly achieves the desired pattern for at least four-fold changes in the size of the swarm, and (ii) compactness (e_L^{ss}) improves as N increases.

4.4 Comparison with [20, 21]

We compared our control law (7) to the so-called “gravitational virtual forces strategy” (see the Appendix) [20, 21], that represent an established solution to geometric pattern formation problems. In [20, 21], a second order damped dynamics is considered for the agents. Hence, for the sake of comparison, we reduced that model to the first order model in (6), by assuming that the viscous friction force is significantly larger than the inertial one.

To select the gravitational gain G and the saturation value F_{max} in the control law from [20, 21], we applied the same tuning procedure described in Sec. 4.2. In particular, we considered $(G, F_{\text{max}}) \in \{0, 0.5, \dots, 10\} \times \{0, 1, \dots, 40\}$, and performed 30 trials for each pair of parameters, obtaining as optimal

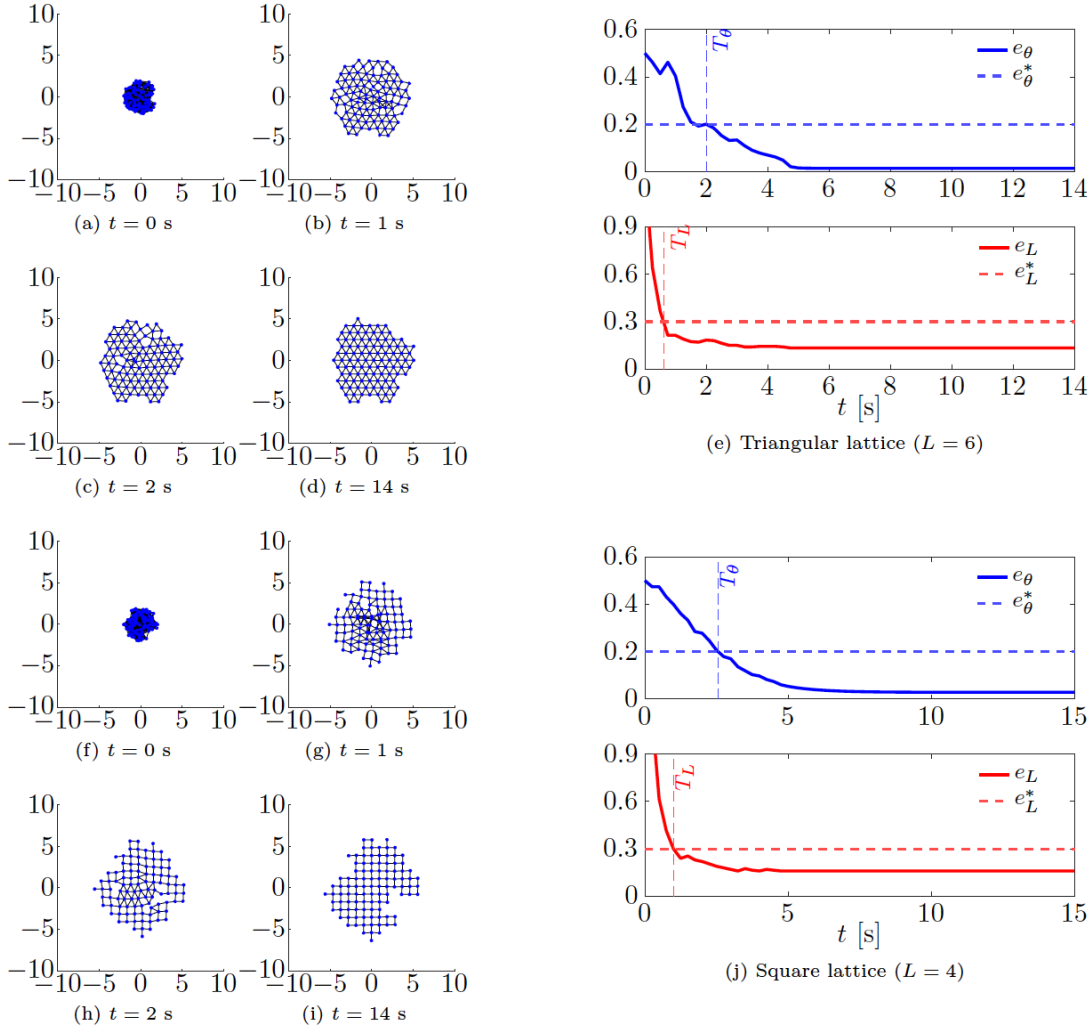


Figure 5: Snapshots at different time instants of a swarm forming (a)–(d) a triangular lattice (f)–(i) and a square lattice (§ 4.2). Panels e and j show the time evolution of the metrics e_θ and e_L for the cases that $L = 6$ and $L = 4$, respectively. When $L = 6$, we set $(G_r, G_n) = (G_r^*, G_n^*)_{L=6}$; when $L = 4$, we set $(G_r, G_n) = (G_r^*, G_n^*)_{L=4}$.

pair for the square lattice $(G^*, F_{\max}^*) = (35, 2)$ (see Fig. 10). All other parameters were kept to the default values in Tab. 2.

Then, we performed the same scalability test in Sec. 4.3.4 and report the results in Fig. 11. Remarkably, by comparing these results with those in the

previous Fig. 9b, we see that our proposed control strategy performs better, obtaining much smaller values of e_θ^{ss} , regardless of the size N of the swarm. In particular, the control law from [20, 21] only rarely achieves $e_\theta^{ss} \leq e_\theta^*$, implying a low success rate.

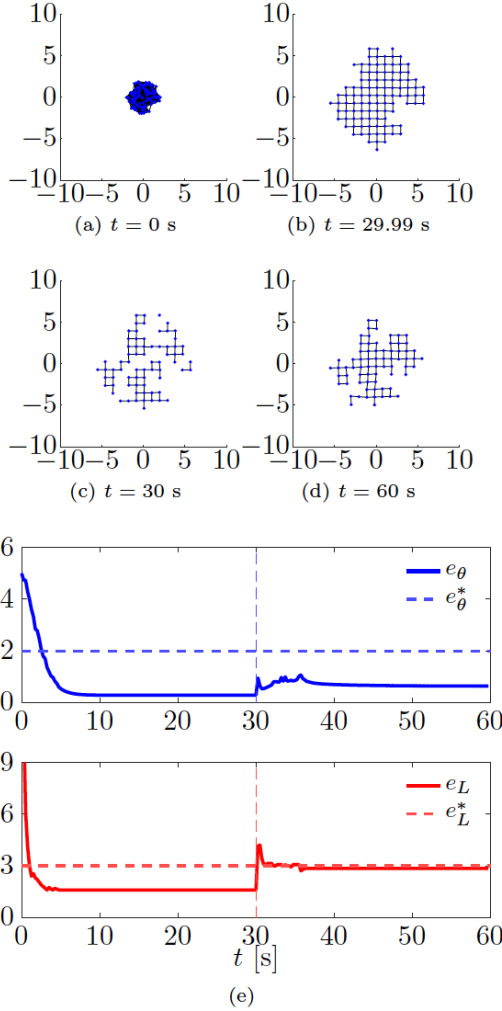


Figure 6: Robustness to removal of agents (§ 4.3.1). Panels a–d show snapshots at different time instants. Panel e shows the time evolution of the metrics; dashed vertical lines denote the time instant when agents are removed. $L = 4$, $(G_r, G_n) = (G_r^*, G_n^*)_{L=4}$.

5 Adaptive tuning of control gains

Tuning the control gains (here $G_{r,i}$ and $G_{n,i}$) can in general be a tedious and time-consuming procedure. Therefore, to avoid it, we propose the use of a simple adaptive control law, that might also improve the ro-

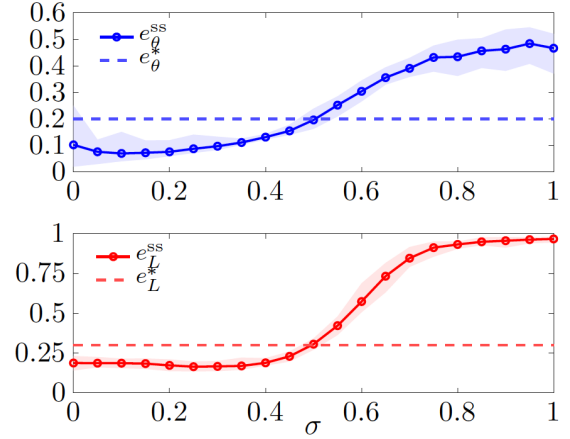


Figure 7: Robustness to noise (§ 4.3.2). e_L^{ss} e e_θ^{ss} , averaged over $M = 30$ trials, varying the standard deviation of the Gaussian noise. The shaded areas represent the maximum and minimum values obtained over the M trials. $L = 4$, $(G_r, G_n) = (G_r^*, G_n^*)_{L=4}$.

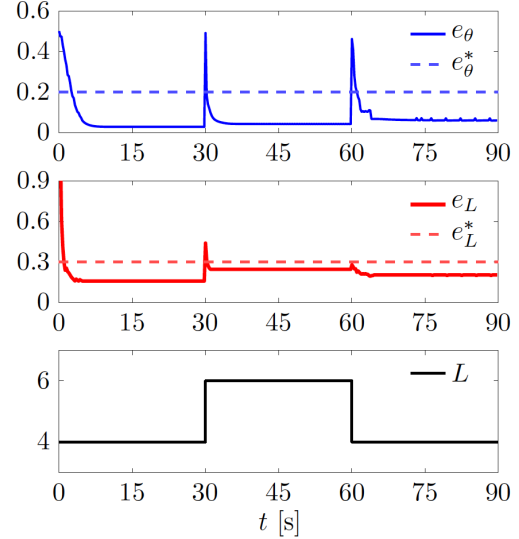
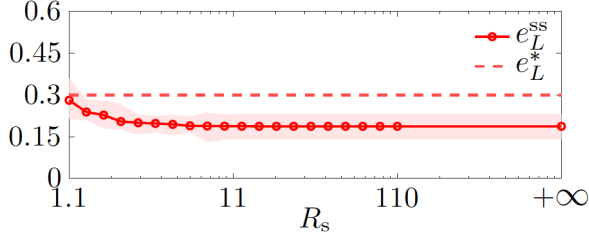
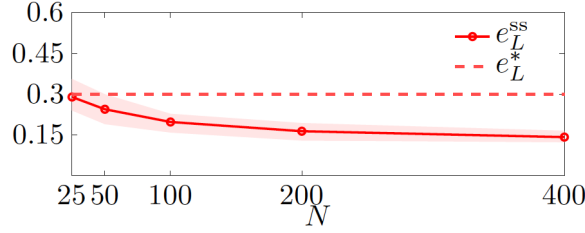
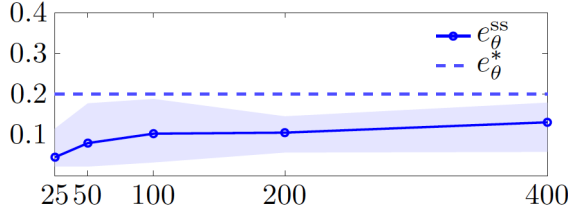


Figure 8: Flexibility to spatial reorganisation (§ 4.3.3). Time evolution of the metrics as L changes. $(G_r, G_n) = (G_r^*, G_n^*)_{L=4}$.

bustness and flexibility of the swarm. Specifically, for the sake of simplicity, $G_{r,i}$ is set to a constant value G_r for all the swarm, while each agent computes its



(a)



(b)

Figure 9: Scalability (§ 4.3.4). (a) e_L^{ss} averaged over $M = 30$ trials with varying R_s . (b) e_θ^{ss} and e_L^{ss} averaged over the trials, with varying N ; $R_s = 3\text{m}$; agents' initial positions are drawn with uniform distribution from a disk with radius $r = \sqrt{N}/25$. The shaded areas represent the maximum and minimum values over the M trials. $L = 4$, $(G_r, G_n) = (G_r^*, G_n^*)_{L=4}$.

gain $G_{n,i}$ independently, using only local information. Letting $e_{\theta,i} \in [0, 1]$ be the *average angular error* for agent i , given by

$$e_{\theta,i} := \frac{L}{\pi} \frac{1}{|\mathcal{A}_i|} \sum_{j \in \mathcal{A}_i} |\theta_{ij}^{\text{err}}|, \quad (20)$$

$G_{n,i}$ is varied according to the law

$$\frac{d}{dt} G_{n,i}(t) = \begin{cases} \alpha (e_{\theta,i}(t) - e_\theta^*), & \text{if } e_{\theta,i}(t) > e_\theta^*, \\ 0, & \text{otherwise.} \end{cases} \quad (21a)$$

$$G_{n,i}(0) = 0, \quad (21b)$$

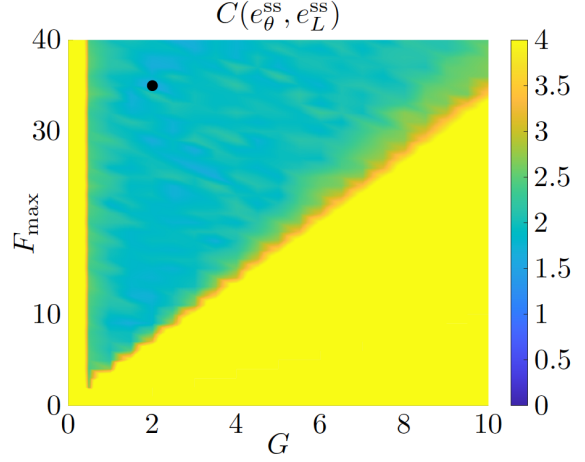


Figure 10: Tuning of parameters G and F_{\max} from [21] (§ 4.4). The black dot denotes the optimal pair (G^*, F_{\max}^*) . $L = 4$.

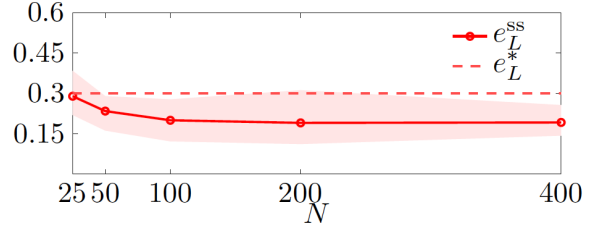
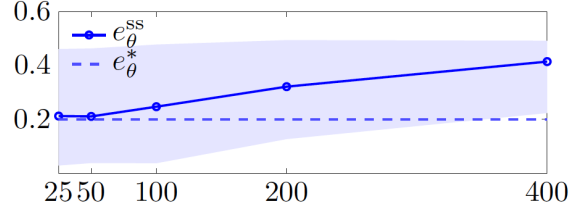


Figure 11: Scalability test for the algorithm from [21] (§ 4.4). e_L^{ss} and e_θ^{ss} averaged over $M = 30$ trials, as N varies. Agents' initial positions are drawn with uniform distribution from a disk of radius $r = \sqrt{N}/25$. The shaded area represents the maximum and minimum values over the trials. $L = 4$, $(G, F_{\max}) = (G^*, F_{\max}^*)$.

where $\alpha > 0$ is an adaptation gain and e_θ^* (introduced in §4.1) is used to determine the amplitude of the dead-zone. Here, we empirically choose $\alpha = 3$. To evaluate the effect of the adaptation law, we also define the average normal gain of the swarm

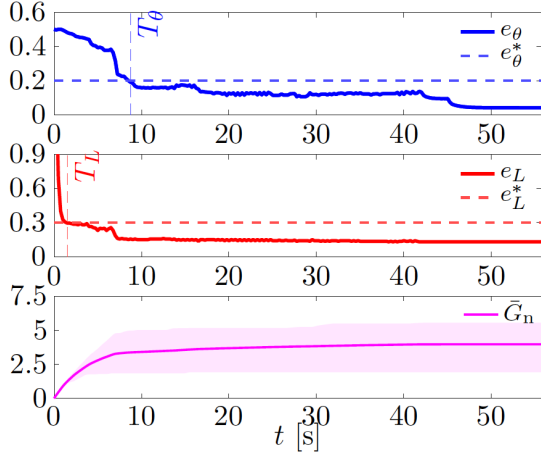


Figure 12: Pattern formation using the adaptive tuning law (21) (§ 5). Initial conditions are the same as those of the simulation in Fig. 5. The shaded magenta area is delimited by $\max_{i \in \mathcal{S}} G_{n,i}$ and $\min_{i \in \mathcal{S}} G_{n,i}$. $L = 4$, $G_r = 15$.

$$\bar{G}_n(t) := \frac{1}{N} \sum_{i=1}^N G_{n,i}(t).$$

In Fig. 12, we report the time evolution of e_L , e_θ , and of \bar{G}_n for a representative simulation. First, we notice that the average normal gain \bar{G}_n eventually settles to a constant value. Moreover, comparing the results with the case in which the gains $G_{n,i}$ are not chosen adaptively (see Sec 4.2 and Fig. 5j, here T_θ , T_L and t_{ss} are larger (meaning longer convergence time) but e_θ^{ss} and e_L^{ss} are smaller (meaning better regularity and compactness performance)).

5.1 Robustness analysis

Next, we test robustness to faults, flexibility, and scalability for the adaptive law (21), similarly to what we did in Sec. 4.3.

5.1.1 Robustness to faults

We ran a series of agent removal tests, as described in Sec. 4.3.1. For the sake of brevity, we report the results of one of such tests with $L = 4$ in Fig. 13. At $t = 30$ s, 30% of the agents are removed; yet, after a short time the swarm reaggregates to recover the desired lattice.

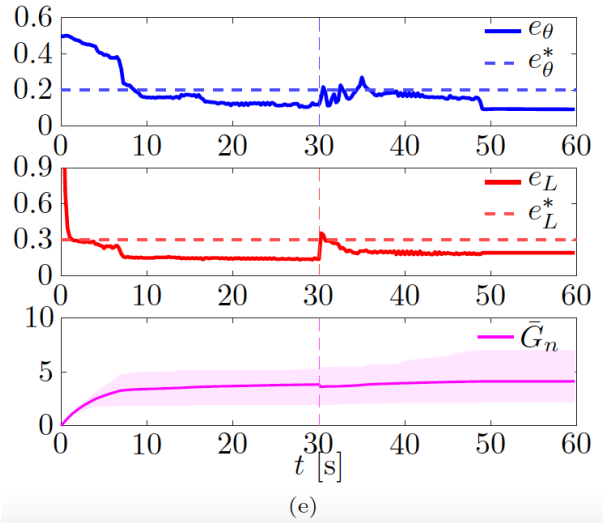
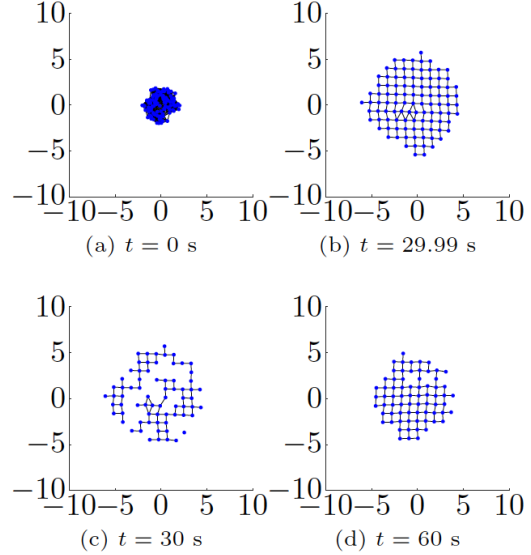


Figure 13: Robustness to agents removal using the adaptive tuning law (21) (§ 5.1.1). Initial conditions are the same as those of the simulation in Fig. 6. Panels a–d show snapshots at different time instants. Panel e shows the time evolution of the metrics; dashed vertical lines denote the time instant when agents are removed. The shaded magenta area is delimited by $\max_{i \in \mathcal{S}} G_{n,i}$ and $\min_{i \in \mathcal{S}} G_{n,i}$. $L = 4$, $G_r = 15$.

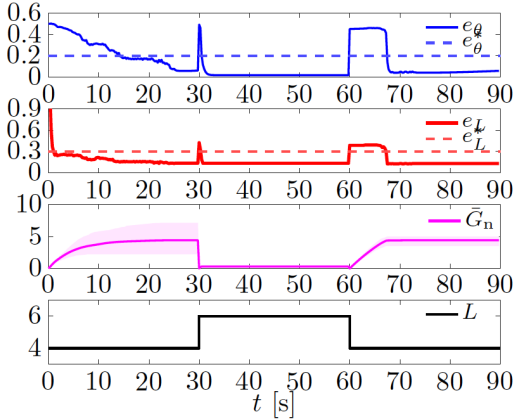


Figure 14: Flexibility using the adaptive tuning law (21) (§ 5.1.2). Initial conditions are the same as those of the simulation in Fig. 8. The shaded magenta area is delimited by $\max_{i \in \mathcal{S}} G_{n,i}$ and $\min_{i \in \mathcal{S}} G_{n,i}$.

5.1.2 Flexibility

We repeated the test in Sec. 4.3.3, with the difference that this time we set $G_r = 18.5$ (that is the average between the optimal gain for square and triangular patterns), and set $G_{n,i}$ according to law (21), resetting all $G_{n,i}$ to 0 when L is changed. The results are shown in Fig. 14. When compared to the non-adaptive case (Fig. 8), here e_θ^{ss} and e_L^{ss} are smaller (better pattern formation), but T_θ and T_L are larger (slower), especially when forming square patterns. Interestingly, when $L = 4$, \bar{G}_n settles to about 5, while when $L = 6$ it settles to about 0.3, a much smaller value.

5.1.3 Scalability

We repeated the test in Sec. 4.3.4, setting again the sensing radius R_s to 3 m and assessing performance while varying the size N of the swarm; results are shown in Fig. 15. First, we notice that the larger the swarm is, the larger the steady state value of \bar{G}_n is. Comparing the results with those of the static gains, in Fig. 9b, here we observe a slight improvement of performance, with a slightly smaller e_θ^{ss} .

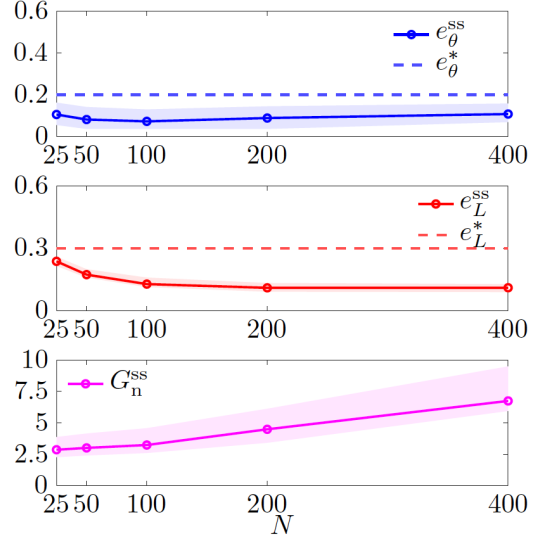


Figure 15: Scalability using the adaptive tuning law (21) (§ 5.1.3). e_θ^{ss} and e_L^{ss} are averaged over $M = 30$ trials with varying N . $R_s = 3$ m; agents' initial positions are drawn with uniform distribution from a disk with radius $r = \sqrt{N/25}$. $G_n^{\text{ss}} := \bar{G}_n(t_{\text{ss}})$. The shaded areas represent the maximum and minimum values over the trials. $L = 4$, $G_r = 15$.

6 Robotarium Experiments

To further validate our control algorithm, we tested it in a real robotic scenario, using the open access *Robotarium* platform [36, 37]. The experimental setup features 20 differential drive robots (GRITSBot [38]), that can move in a 3.2 m \times 2 m rectangular arena. The robots have a diameter of about 11 cm, a maximum (linear) speed of 20 cm/s, and a maximum rotational speed of about 3.6 rad/s. To cope with the limited size of the arena, distances $\|\mathbf{r}_{ij}\|$ in (9) are doubled, while control inputs \mathbf{u}_i are halved. The Robotarium implementation includes a collision avoidance safety protocol and transforms the velocity inputs (7) into appropriate acceleration control inputs for the robots. Moreover, we run an initial routine to yield an initial condition in which the agents are aggregated as much as possible at the centre, similarly to what considered in Sec. 4.

As a paradigmatic example, we performed a flexibility test (similarly to what done in Sec 4.3.3 and

reported in Fig. 8). During the first 33 seconds, the agents reach an aggregated initial condition. Then we set $L = 4$ for $t \in [33, 165)$, $L = 6$ for $t \in [165, 297)$, and $L = 4$ for $t \in [297, 429]$, ending the simulation. We used the static control law (7)-(8) and (11), and to comply with the limited size of the arena, we scaled the control gains to the values $G_r = 0.8$ and $G_n = 0.4$, selected empirically.

The resulting movie is available online (<https://github.com/diBernardoGroup/SwarmSimPublic>), while representative snapshots are reported in Fig. 16, with the time evolution of the metrics. The metrics qualitatively reproduce the behaviour obtained in simulation (see Fig. 8). In particular, we obtain $e_\theta^{ss} < e_\theta^*$, with both triangular and square patterns. On the other hand, we obtain $e_L^{ss} < e_L^*$ when forming square patterns, but $e_L^{ss} > e_L^*$ with triangular patterns; this is a consequence of the relatively small swarm size, and does not mean that the pattern is not achieved, as it can be seen in Fig. 16.(c) showing the pattern is successfully achieved.

7 Conclusions

We presented a distributed control law to solve pattern formation for the case of square and triangular lattices, based on the use of virtual forces. Our control strategy is distributed, only requires distance sensors and a compass, and does not need communication between the agents. We showed via exhaustive simulations and experiments that the strategy is effective in achieving triangular and square lattice; we also compared it the distance-based strategy in [21], observing better performance particularly when the goal is that of achieving square lattices. Additionally, we showed that the control law is robust to failures of the agents, to noise, is flexible to changes in the lattice and scalable with respect to the number of agents. We also presented a simple yet effective adaptive law to automatically tune the gains so as to be able to switch the goal pattern in real-time.

In the future, we plan to study analytically the stability and convergence of the control law. Additionally, we will investigate the extension to other patterns (e.g. hexagonal ones) and a more sophisti-

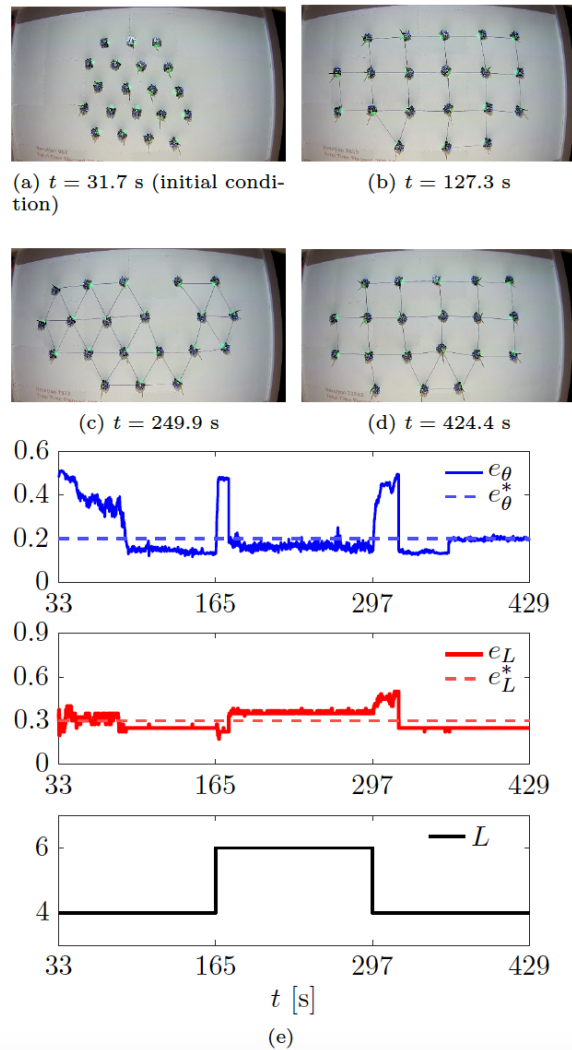


Figure 16: Flexibility test in Robotarium (§ 6). Panels a–d show the swarm at different time instants. Panel e shows the time evolution of the metrics and the parameter L . $(G_r, G_n) = (G_r^*, G_n^*)_{L=4}$.

cated adaptive law able to tune all the control gains at the same time.

A The algorithm from [20, 21] References

Let us first introduce some useful notation. Given a real-valued function $x(t)$ and $a, b \in \mathbb{R}$ with $a < b$, we introduce the *saturation* of $x(t)$ between a and b , given by

$$[x(t)]_a^b := \begin{cases} a, & \text{if } x(t) < a, \\ x(t), & \text{if } a \leq x(t) \leq b, \\ b, & \text{if } x(t) > b. \end{cases}$$

In [20, 21, 31], the agent dynamics is described by

$$\begin{cases} \dot{\mathbf{x}}_i = \mathbf{v}_i, \\ \dot{\mathbf{v}}_i = \frac{1}{m}(\mathbf{u}_i - \mu \mathbf{v}_i), \end{cases} \quad \forall i \in \mathcal{S}, \quad (22)$$

where $\mathbf{u}_i \in \mathbb{R}^2$ is the control input, $m \in \mathbb{R}_{>0}$ is the mass of the agent and $\mu \in \mathbb{R}_{>0}$ is the friction damping factor. Recall that, as described in Sec. 3.1, under a few assumptions, (22) can be recast as (6). The control input \mathbf{u}_i is given by

$$\mathbf{u}_i = \sum_{j=1}^N f(\|\mathbf{r}_{ij}\|) \frac{\mathbf{r}_{ij}}{\|\mathbf{r}_{ij}\|}, \quad (23)$$

where f is a gravitational-like virtual force, given by

$$f(\|\mathbf{r}_{ij}\|) = \begin{cases} \left[G \frac{m^2}{\|\mathbf{r}_{ij}\|^2} \right]_0^{F_{\max}}, & \text{if } 0 \leq \|\mathbf{r}_{ij}\| \leq R, \\ - \left[G \frac{m^2}{\|\mathbf{r}_{ij}\|^2} \right]_0^{F_{\max}}, & \text{if } R < \|\mathbf{r}_{ij}\| \leq 1.5R, \\ 0, & \text{otherwise.} \end{cases} \quad (24)$$

In (24), $G, F_{\max} \in \mathbb{R}_{\geq 0}$ are tunable control gains, and $R \in \mathbb{R}_{>0}$.

The control law given by (23) and (24) was showed to work for triangular lattices. To make it suitable for square patterns, a binary variable called *spin* is introduced for each agent, and the swarm is divided in two subsets, depending on the value of their spin. Then, agents with different spin aggregate at a distance of R , while agents with the same spin do so at a distance of $\sqrt{2}R$. The extension to the case of hexagonal lattice is discussed in [31] and requires communication among the agents.

- [1] Gregory Dudek, Michael R.M. Jenkin, Evangelos Milios, and David Wilkes. A taxonomy for multi-agent robotics. *Autonomous Robots*, 3(4):375–397, 1996.
- [2] Fabrizia Auletta, Davide Fiore, Michael J. Richardson, and Mario di Bernardo. Herding stochastic autonomous agents via local control rules and online target selection strategies. *Autonomous Robots*, 46(3):469–481, 2022.
- [3] Levent Bayindir. A review of swarm robotics tasks. *Neurocomputing*, 172:292–321, 2016.
- [4] Manuele Brambilla, Eliseo Ferrante, Mauro Biorattari, and Marco Dorigo. Swarm robotics: a review from the swarm engineering perspective. *Swarm Intelligence*, 7(1):1–41, 2013.
- [5] Sabine Hauert, Jean Christophe Zufferey, and Dario Floreano. Evolved swarming without positioning information: An application in aerial communication relay. *Autonomous Robots*, 26(1):21–32, 2009.
- [6] Michael Rubenstein, Alejandro Cornejo, and Radhika Nagpal. Programmable self-assembly in a thousand-robot swarm. *Science*, pages 795–799, 2014.
- [7] Gaurav Gardi, Steven Ceron, Wendong Wang, Kirstin Petersen, and Metin Sitti. Microrobot collectives with reconfigurable morphologies, behaviors, and functions. *Nature Communications*, 13(1):1–14, 2022.
- [8] Hyondong Oh, Ataollah Ramezan Shirazi, Chaoli Sun, and Yaochu Jin. Bio-inspired self-organising multi-robot pattern formation: A review. *Robotics and Autonomous Systems*, 91:83–100, 2017.
- [9] Haitao Zhao, Jibo Wei, Shengchun Huang, Li Zhou, and Qi Tang. Regular topology formation based on artificial forces for distributed mobile robotic networks. *IEEE Transactions on Mobile Computing*, 18(10):2415–2429, 2018.

- [10] Seungkeun Kim, Hyondong Oh, Jinyoung Suk, and Antonios Tsourdos. Coordinated trajectory planning for efficient communication relay using multiple UAVs. *Control Engineering Practice*, 29:42–49, 2014.
- [11] El Mane Wong, Frédéric Bourgault, and Tomonari Furukawa. Multi-vehicle Bayesian search for multiple lost targets. In *Proceedings of the IEEE International Conference on Robotics and Automation*, volume 2005, pages 3169–3174. IEEE, 2005.
- [12] Jim Pugh and Alcherio Martinoli. Inspiring and modeling multi-robot search with particle swarm optimization. In *Proceedings of the 2007 IEEE Swarm Intelligence Symposium (SIS 2007)*, pages 332–339. IEEE, 2007.
- [13] Michael Rubenstein, Adrian Cabrera, Justin Werfel, Golnaz Habibi, James McLurkin, and Radhika Nagpal. Collective transport of complex objects by simple robots. In *Proceedings of the 2013 International Conference on Autonomous Agents and Multi-agent Systems*, pages 47–54, 2013.
- [14] John G. Mooney and Eric N. Johnson. A Comparison of Automatic Nap-of-the-earth Guidance Strategies for Helicopters. *Journal of Field Robotics*, 31(4):637–653, 2014.
- [15] Sebastian Thrun, Wolfram Burgard, and Dieter Fox. Real-time algorithm for mobile robot mapping with applications to multi-robot and 3D mapping. In *Proceedings of the 2000 IEEE International Conference on Robotics and Automation*, volume 1, pages 321–328, 2000.
- [16] Kwang Kyo Oh, Myoung Chul Park, and Hyo Sung Ahn. A survey of multi-agent formation control. *Automatica*, 53:424–440, 2015.
- [17] Jorge Cortés. Global and robust formation-shape stabilization of relative sensing networks. *Automatica*, 45(12):2754–2762, 2009.
- [18] Carlo Pinciroli, Mauro Birattari, Elio Tuci, Marco Dorigo, Marco Del Rey Zapatero, Tamas Vinko, and Dario Izzo. Self-organizing and scalable shape formation for a swarm of pico satellites. In *Proceedings of the 2008 NASA/ESA Conference on Adaptive Hardware and Systems (AHS 2008)*, pages 57–61, 2008.
- [19] Arnaud Casteigts, Jérémie Albert, Serge Chaumette, Amiya Nayak, and Ivan Stojmenovic. Biconnecting a network of mobile robots using virtual angular forces. *Computer Communications*, 35(9):1038–1046, 2012.
- [20] William M. Spears and Diana F. Gordon. Using artificial physics to control agents. In *Proceedings of the 1999 International Conference on Information Intelligence and Systems (ICIIS 1999)*, pages 281–288. IEEE, 1999.
- [21] William M. Spears, Diana F. Spears, Jerry C. Hamann, and Rodney Heil. Distributed, physics-based control of swarms of vehicles. *Autonomous Robots*, 17(2):137–162, 2004.
- [22] Suranga Hettiarachchi and William M. Spears. Moving swarm formations through obstacle fields. In *Proceedings of the 2005 International Conference on Artificial Intelligence (ICAI’05)*, pages 97–103, 2005.
- [23] Salvatore Torquato. Inverse optimization techniques for targeted self-assembly. *Soft Matter*, 5(6):1157–1173, 2009.
- [24] Xiang Li, M. Fikret Ercan, and Yu Fai Fung. A triangular formation strategy for collective behaviors of robot swarm. In *Proceedings of the 2009 International Conference on Computational Science and Its Applications (ICCSA 2009)*, pages 897–911. Springer, 2009.
- [25] Geunho Lee and Nak Young Chong. A geometric approach to deploying robot swarms. *Annals of Mathematics and Artificial Intelligence*, 52(2):257–280, 2008.
- [26] Tucker Balch and Maria Hybinette. Social potentials for scalable multi-robot formations. In

- Proceedings of the IEEE International Conference on Robotics and Automation (ICRA 2000)*, volume 1, pages 73–80, 2000.
- [27] Tucker Balch and Maria Hybinette. Behavior-based coordination of large-scale robot formations. In *Proceedings of the 4th International Conference on MultiAgent Systems (ICMAS 2000)*, pages 363–364, 2000.
- [28] Yang Song and Jason M. O’Kane. Decentralized formation of arbitrary multi-robot lattices. In *Proceedings of the IEEE International Conference on Robotics and Automation (ICRA 2014)*, pages 1118–1125. IEEE, 2014.
- [29] Oussama Khatib. Real-time obstacle avoidance for manipulators and mobile robots. In *Proceedings of the IEEE International Conference on Robotics and Automation (ICRA 85)*, pages 500–505. IEEE, 1985.
- [30] M. R. D’Orsogna, Y. L. Chuang, A. L. Bertozzi, and L. S. Chayes. Self-propelled particles with soft-core interactions: Patterns, stability, and collapse. *Physical Review Letters*, 96(10):104302, 2006.
- [31] Prabhu Sailesh, Li William, and McLurkin James. Hexagonal lattice formation in multi-robot systems. *Distributed Autonomous Robotic Systems*, 104:307–320, 2014.
- [32] Geunho Lee, Yasuhiro Nishimura, Kazutaka Tataru, and Nak Young Chong. Three dimensional deployment of robot swarms. In *Proceedings of the IEEE/RSJ 2010 International Conference on Intelligent Robots and Systems (IROS 2010)*, pages 5073–5078. IEEE, 2010.
- [33] Vito Latora, Vincenzo Nicosia, and Giovanni Russo. *Complex Networks: Principles, Methods and Applications*. Cambridge University Press, 2017.
- [34] Branko Grünbaum and Geoffrey C. Shephard. Tilings by Regular Polygons. *Mathematics Magazine*, 50(5):227–247, 1977.
- [35] Peter Engel, Louis Michel, and Marjorie Senechal. Lattice Geometry. Technical report, Institut des Hautes Etudes Scientifique, 2004.
- [36] Daniel Pickem, Paul Glotfelter, Li Wang, Mark Mote, Aaron Ames, Eric Feron, and Magnus Egerstedt. The Robotarium: A remotely accessible swarm robotics research testbed. In *Proceedings of the IEEE International Conference on Robotics and Automation (ICRA 2017)*, pages 1699–1706. IEEE, 2017.
- [37] S. Wilson, P. Glotfelter, L. Wang, S. Mayya, G. Notomista, M. Mote, and M. Egerstedt. The Robotarium: Globally Impactful Opportunities, Challenges, and Lessons Learned in Remote-Access, Distributed Control of Multi-robot Systems. *IEEE Control Systems Magazine*, 40(1):26–44, 2020.
- [38] Daniel Pickem, Myron Lee, and Magnus Egerstedt. The GRITSBot in its natural habitat - A multi-robot testbed. In *Proceedings of the IEEE International Conference on Robotics and Automation (ICRA 2015)*, volume 2015-June, pages 4062–4067, 2015.